Magnetic properties of stage-2 $Ni_cMn_{1-c}Cl_2$-graphite intercalation compounds

Itsuko S. Suzuki, Floyd Khemai, Masatsugu Suzuki, and Charles R. Burr
Department of Physics and Materials Research Center, State University of New York at Binghamton, Binghamton, New York 13902-6000
(Received 7 August 1991)

Stage-2 $Ni_cMn_{1-c}Cl_2$-graphite intercalation compounds (with $0 \le c \le 1$) are two-dimensional random-spin systems with competing ferromagnetic and antiferromagnetic exchange interactions. The magnetic properties of these compounds have been studied by dc and ac magnetic susceptibilities. The Curie-Weiss temperature increases monotonically with increasing Ni concentration, suggesting that both Ni and Mn ions are randomly distributed on the triangular-lattice sites of the $Ni_cMn_{1-c}Cl_2$-intercalate layers. Its sign changes from negative to positive around $c \approx 0.22$. The exchange interaction between Ni-Mn spin pairs is ferromagnetic and is described by $J(\text{Ni-Mn}) = 1.09[|J(\text{Ni-Ni})J(\text{Mn-Mn})|]^{1/2} = 1.44$ K. The critical temperature T_c decreases rapidly with a dilution of Mn. In spite of ferromagnetic J(Ni-Mn), the ferromagnetic long-range order of Ni^{2+} disappears below $c \approx 0.6$. The large initial slope of $[d\ln T_c/dc]_{c=1} = 2.38$ is ascribed to the two-dimensional Heisenberg-like character of stage-2 $NiCl_2$-graphite intercalation compound. The critical behavior of these compounds shows a two-dimensional XY character. The critical exponent γ appears to be independent of c for $c \ge 0.7$: It is determined that $\gamma = 2.27 \pm 0.02$ at $c = 0.9$.

I. INTRODUCTION

Recently, the magnetic properties of random-mixture graphite intercalation compounds (RMGIC's) have received considerable interest.[1-5] The magnetic RMGIC's provide a variety of opportunities to study magnetic phase transitions of two-dimensional (2D) random-spin systems. There have been several studies of the magnetic properties of magnetic RMGIC's: stage-2 $Co_cNi_{1-c}Cl_2$ GIC's,[1,2] stage-1 $Co_cMg_{1-c}Cl_2$ GIC's,[3] and stage-2 $Co_cMn_{1-c}Cl_2$ GIC's,[4,5] where c is the Co concentration ($0 \le c \le 1$). Yeh *et al.*[1,2] succeeded in synthesizing stage-2 $Co_cNi_{1-c}Cl_2$ GIC samples and reported the results of the dc magnetic susceptibility. These compounds have ferromagnetic intraplanar exchange interactions between Co-Co spin pairs and between Ni-Ni spin pairs. Nicholls and Dresselhaus[3] have studied the magnetic phase transition of stage-1 $Co_cMg_{1-c}Cl_2$ GIC's from the temperature and field dependences of the ac magnetic susceptibility. In these compounds a part of the Co^{2+} ions on the triangular-lattice sites is replaced by nonmagnetic Mg^{2+} ions. Suzuki *et al.*[4,5] have studied the magnetic properties of stage-2 $Co_cMn_{1-c}Cl_2$ GIC's, where the intraplanar exchange interaction between Co-Co spin pairs is ferromagnetic, but the intraplanar exchange interaction between Mn-Mn spin pairs is antiferromagnetic.

The magnetic behavior of stage-2 $Ni_cMn_{1-c}Cl_2$ GIC's seems to be similar to that of stage-2 $Co_cMn_{1-c}Cl_2$ GIC's. The spin-frustration effect is expected to occur because of the competition between ferromagnetic intraplanar interactions between Ni-Ni spin pairs and antiferromagnetic intraplanar interactions between Mn-Mn spin pairs. In this paper we study the magnetic properties and magnetic phase transitions of stage-2 $Ni_cMn_{1-c}Cl_2$ GIC's by using dc and ac magnetic susceptibility. The Curie-Weiss temperature, effective magnetic moment, and critical temperature will be determined as a function of Ni concentration. The magnetic phase diagram of these compounds will be discussed in comparison with that of stage-2 $Co_cMn_{1-c}Cl_2$ GIC's.[5]

There have been several studies on the magnetic properties of the stage-2 $NiCl_2$ GIC (Refs. 6–8) and stage-2 $MnCl_2$ GIC.[9-11] The stage-2 $NiCl_2$ GIC magnetically behaves like a 2D Heisenberg ferromagnet with small XY anisotropy on the triangular-lattice sites. The spin Hamiltonian of Ni^{2+} ions is described by

$$\mathcal{H} = -2J \sum_{\langle i,j \rangle} \mathbf{S}_i \cdot \mathbf{S}_j + D \sum_i (S_i^z)^2 + 2J' \sum_{\langle i,m \rangle} \mathbf{S}_i \cdot \mathbf{S}_m \ , \qquad (1)$$

where z axis coincides with the c axis, $\langle i,j \rangle$ denotes nearest-neighbor pairs on the same intercalate layer, $\langle i,m \rangle$ denotes nearest-neighbor pairs on the adjacent intercalate layer, S is the spin of Ni^{2+} [$S(\text{Ni}) = 1$], J is the intraplanar exchange interaction [$J(\text{Ni-Ni}) = 8.75$ K], D is a single-ion anisotropy parameter [$D(\text{Ni}) = 0.80$ K], and J' is the antiferromagnetic interplanar exchange interaction ($|J'|/J \approx 10^{-3}$). The magnetic and structural data of this compound are listed in Table I. This compound shows two magnetic phase transitions at $T_{cu} = 22.0$ K and $T_{cl} = 17.5$ K. Above T_{cu} the system is in the paramagnetic phase. In the intermediate phase between T_{cl} and T_{cu}, the system has 2D spin ordering. There is no spin correlation between adjacent $NiCl_2$ layers. Below T_{cl} there occurs the 3D antiferromagnetic phase where 2D ferromagnetic layers are antiferromagnetically stacked along the c axis. The stage-2 $MnCl_2$ GIC magnetically behaves like a 2D XY-like antiferromagnet on the triangular-lattice sites. The spin Hamiltonian of Mn^{2+} ions is expressed by the same form as Eq. (1) with spin $S(\text{Mn}) = \frac{5}{2}$, antiferromagnetic intraplanar exchange

TABLE I. Structural and magnetic properties of the stage-2 $NiCl_2$ GIC and $MnCl_2$ GIC, where g is the g factor along the c plane, a is the in-plane lattice constant, and d is the c-axis repeat distance.

Stage-2 $NiCl_2$ GIC		Stage-2 $MnCl_2$ GIC	
S	1	S	5/2
J (K)	8.75	J (K)	−0.20
D (K)	0.80	D (K)	0.97
T_{cl} (K)	17.5	T_N (K)	1.1
T_{cu} (K)	22.0		
Θ (K)	69.28	Θ (K)	−10.19
$P(\mu_B)$	3.19	$P(\mu_B)$	6.04
g	2.26	g	2.04
d (Å)	12.70	d (Å)	12.89
a (Å)	3.46	a (Å)	3.67

interaction J(Mn-Mn)$=-0.20$ K, and single-ion anisotropy D(Mn)$=0.97$ K. The magnetic and structural data of this compound are shown in Table I. This compound shows a magnetic phase transition at $T_N=1.1$ K. Above T_N it is in the paramagnetic phase. Below T_N it is in the antiferromagnetic phase where all spins lie in the $MnCl_2$ layers.[9-11]

II. EXPERIMENT

Single crystals of $Ni_cMn_{1-c}Cl_2$ were prepared by heating a mixture of c-$NiCl_2$ and $(1-c)$-$MnCl_2$ sealed in vacuum at a reaction temperature 990°C. Stage-2 $Ni_cMn_{1-c}Cl_2$ GIC's were synthesized by heating single-crystal Kish graphites and single-crystal $Ni_cMn_{1-c}Cl_2$ in a chlorine-gas atmosphere at a pressure of 740 Torr. The reaction was continued at 560°C for 20 days. The stoichiometry of the GIC samples listed in Table II was determined from a weight uptake measurement. The dc magnetic susceptibility of stage-2 $Ni_cMn_{1-c}Cl_2$ GIC's was measured by the Faraday balance method in the temperature range between 1.5 and 300 K. A magnetic field of 100 Oe $\le H \le$ 4 kOe was applied in an arbitrary direction in the c plane of the samples. The ac magnetic susceptibility of stage-2 $Ni_cMn_{1-c}Cl_2$ GIC's was measured by a conventional ac Hartshorn bridge method in the temperature range between 2.6 and 25 K. An ac magnetic field of 330 Hz was applied in an arbitrary direction in the c plane of the samples.

III. RESULTS

The dc magnetic susceptibility of stage-2 $Ni_cMn_{1-c}Cl_2$ GIC's with $c=0$, 0.1, 0.15, 0.25, 0.3, 0.35, 0.4, 0.5, 0.65, 0.7, 0.8, 0.85, 0.9, and 1 was measured at $H=4$ kOe in the temperature range $20 \le T \le 300$ K. A least-squares fit of the dc magnetic-susceptibility data for $150 \le T \le 300$ K to the Curie-Weiss law

$$\chi = \frac{C}{T-\Theta} + \chi_0 \tag{2}$$

yields values of the Curie-Weiss constant C (emu K/av. mol), the Curie-Weiss temperature Θ (K), and the temperature-independent susceptibility χ_0 (emu/av. mol). The values of C, Θ, and χ_0 are listed in Table II. Figure 1 shows the reciprocal susceptibility $(\chi-\chi_0)^{-1}$ for $c=0$, 0.3, 0.65, and 0.9 as a function of temperature. The dc magnetic susceptibility is found to obey the Curie-Weiss law above 150 K. The deviation of the reciprocal susceptibility from a straight line below 150 K may indicate the appearance of spin short-range order. The Curie-Weiss temperature Θ vs Ni concentration is shown in Fig. 2. The value of Θ monotonically increases as the Ni concentration increases and changes its sign from negative to positive around $c \approx 0.22$. This implies that the average intraplanar exchange interaction changes from antiferromagnetic to ferromagnetic. According to the molecular-field theory developed by Hashimoto[12] and subsequently modified by Yeh, Suzuki, and Burr,[1] the Curie-Weiss temperature Θ is expressed by

$$\Theta = \frac{c^2P^2(\mathrm{Ni})\Theta(\mathrm{Ni}) + (1-c)^2P^2(\mathrm{Mn})\Theta(\mathrm{Mn}) + 2pc(1-c)\sqrt{|\Theta(\mathrm{Ni})\Theta(\mathrm{Mn})|}P(\mathrm{Ni})P(\mathrm{Mn})}{cP^2(\mathrm{Ni}) + (1-c)P^2(\mathrm{Mn})} , \tag{3}$$

where P(Ni) and P(Mn) are the effective magnetic moments of the stage-2 $NiCl_2$ GIC and $MnCl_2$ GIC, respectively, and Θ(Ni) and Θ(Mn) are the Curie-Weiss temperature of the stage-2 $NiCl_2$ GIC and $MnCl_2$ GIC, respectively (Table I). Here p is a parameter defined by $p=J(\text{Ni-Mn})/[\,|J(\text{Ni-Ni})J(\text{Mn-Mn})|\,]^{1/2}$, where J(Ni-Mn) is the intraplanar exchange interaction between Ni-Mn pairs in the $Ni_cMn_{1-c}Cl_2$ intercalate layer. The data of Θ in Fig. 2 can be fit well by Eq. (3) with $p=1.09$, indicating that J(Ni-Mn) is ferromagnetic and is estimated as 1.44 K. Note that

$$p = J(\text{Co-Mn})/[\,|J(\text{Co-Co})J(\text{Mn-Mn})|\,]^{1/2} = 1.20 ,$$

for stage-2 $Co_cMn_{1-c}Cl_2$ GIC's.[5] We find that J(Ni-Mn) $(=1.44$ K) of stage-2 $Ni_cMn_{1-c}Cl_g$ GIC's is almost the same as J(Co-Mn) $(=1.49$ K) of stage-2 $Co_2Mn_{1-c}Cl_2$ GIC's. Figure 3 shows the average effective magnetic moment P_{eff} of these compounds as a function of Ni concentration. The magnetic moment P_{eff} monotonically decreases with increasing Ni concentration. According to the molecular-field theory,[1] P_{eff} is given by

$$P_{\text{eff}}(c) = [cP^2(\mathrm{Ni}) + (1-c)P^2(\mathrm{Mn})]^{1/2} . \tag{4}$$

The solid line in Fig. 3 denotes the value of P_{eff} described by Eq. (4) with $P(\mathrm{Ni})=3.19\mu_B$/mol and $P(\mathrm{Mn})=6.04\mu_B$/mol. Our data are fit well to the solid line, indicating that (i) the Ni concentration of GIC samples coincides with that of intercalant samples and (ii) Ni and Mn exist as divalent ions in the intercalate layer.

The dc magnetic susceptibility of stage-2 $Ni_cMn_{1-c}Cl_2$

TABLE II. Curie-Weiss temperature Θ and average effective magnetic moment P_{eff} for stage-2 $Ni_cMn_{1-c}Cl_2$ GIC's with the stoichiometry $C_nNi_cMn_{1-c}Cl_2$.

c	n	Θ (K)	P_{eff} (μ_B/av. mol)
0.0	11.03	−10.19±0.77	6.04
0.1	9.50	−6.68±0.26	5.73
0.15	10.99	−4.95±0.43	5.45
0.25	13.57	0.44±0.55	5.35
0.3	13.08	0.04±0.54	5.24
0.35	14.62	7.71±0.46	5.21
0.4	16.83	9.04±0.95	4.85
0.5	12.18	18.07±0.50	4.77
0.65	14.98	24.94±0.28	4.27
0.7	11.95	31.90±0.73	4.23
0.8	14.33	38.49±1.04	4.08
0.85	13.76	42.95±0.58	3.94
0.9	12.03	58.45±0.25	3.48
1	15.37	69.28±0.36	3.19

GIC's with $c=0$, 0.1, 0.15, 0.25, 0.3, 0.35, 0.4, 0.5, 0.65, 0.7, 0.8, 0.85, 0.9, and 1 was measured in the temperature range $1.5 \leq T \leq 25$ K, where an external field **H** (=100 and 840 Oe) is applied along the direction perpendicular to the c axis. Figure 4(a) shows the temperature dependence of M/H at $H=100$ Oe for stage-2 $Ni_cMn_{1-c}Cl_2$ GIC's with $c=0.65$, 0.7, 0.8, 0.9, and 1, where M is the magnetization measured in units of emu/av. mol. The magnetization rapidly decreases with increasing temperature. It does not reduce to zero at a critical temperature T_c, but shows a tail around T_c. This tail is due to the smearing of T_c, which arises from a macroscopic gradient of the Ni concentration over the sample and from the

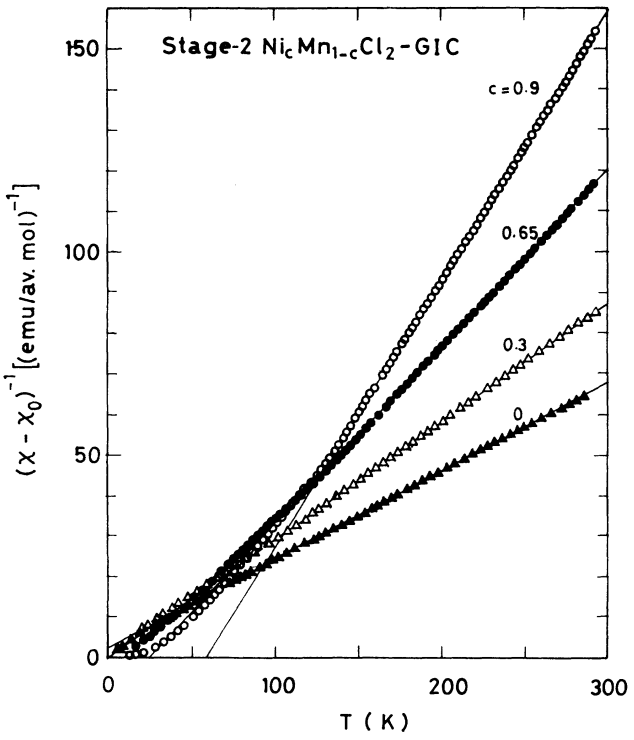

FIG. 1. Reciprocal susceptibility $(\chi-\chi_0)^{-1}$ vs T for stage-2 $Ni_cMn_{1-c}Cl_2$ GIC's with $c=0$ (▲), 0.30 (△), 0.65 (●), and 0.90 (○), where χ_0 is a temperature-independent susceptibility. The solid line is described by Eq. (2) with C, Θ, and χ_0 listed in Table II.

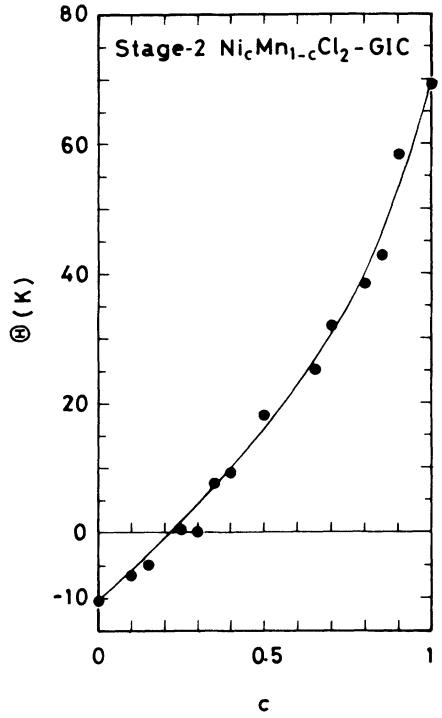

FIG. 2. Curie-Weiss temperature Θ vs c for stage-2 $Ni_cMn_{1-c}Cl_2$ GIC's. The solid line is described by Eq. (3) with $p=1.09$.

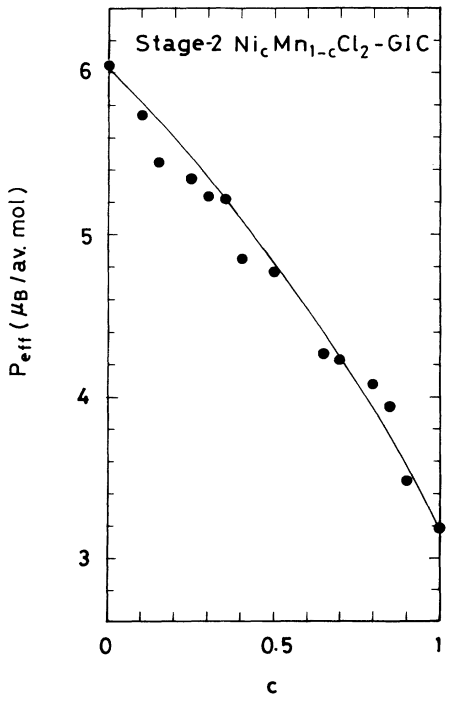

FIG. 3. Average effective magnetic moment P_{eff} (μ_B/av mol) vs c for stage-2 $Ni_cMn_{1-c}Cl_2$ GIC's. The solid line is described by Eq. (4).

finite-size effect of islands.[2] When the distribution of the critical temperature is assumed to be Gaussian with average critical temperature $\langle T_c \rangle$ and width σ, the magnetization can be expressed by a power law, with critical exponent β,

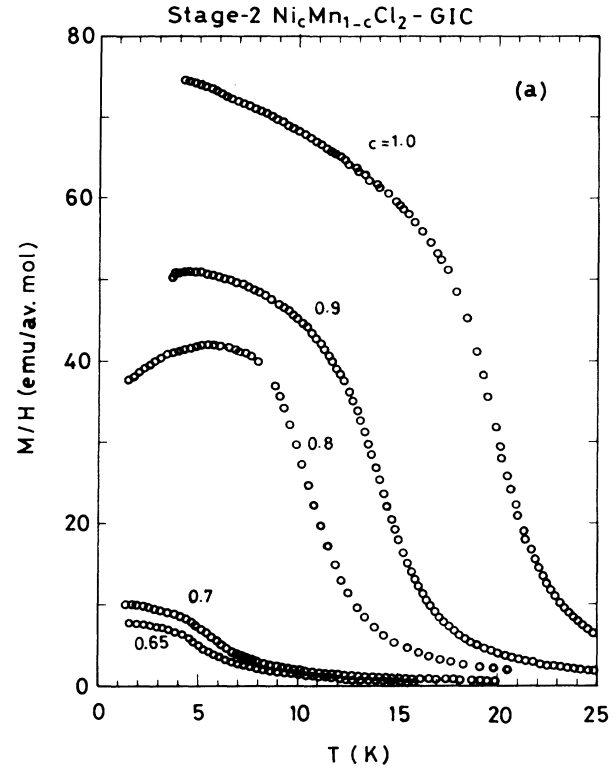

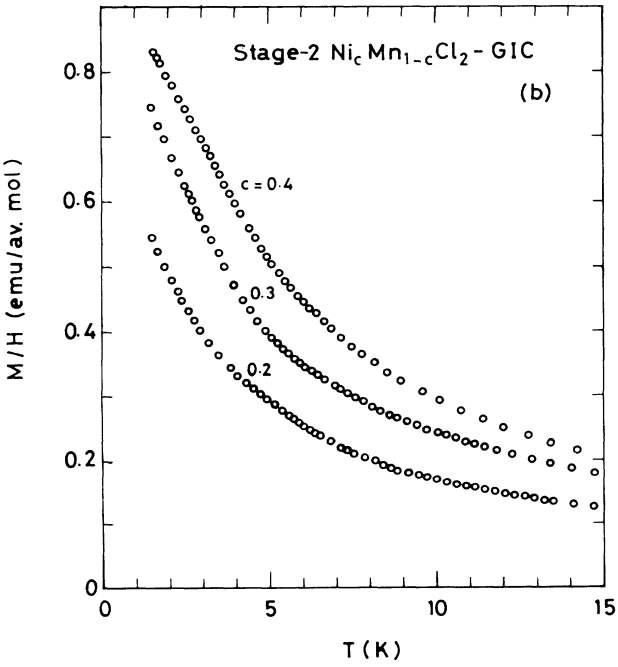

FIG. 4. (a) M/H vs T for stage-2 $Ni_cMn_{1-c}Cl_2$ GIC's with $c=0.65$, 0.7, 0.8, 0.9, and 1, where $H=100$ Oe and $\mathbf{H}\perp c$. (b) M/H vs T for stage-2 $Ni_cMn_{1-c}Cl_2$ GIC's with $c=0.2$, 0.3, and 0.4, where $H=840$ Oe and $\mathbf{H}\perp c$.

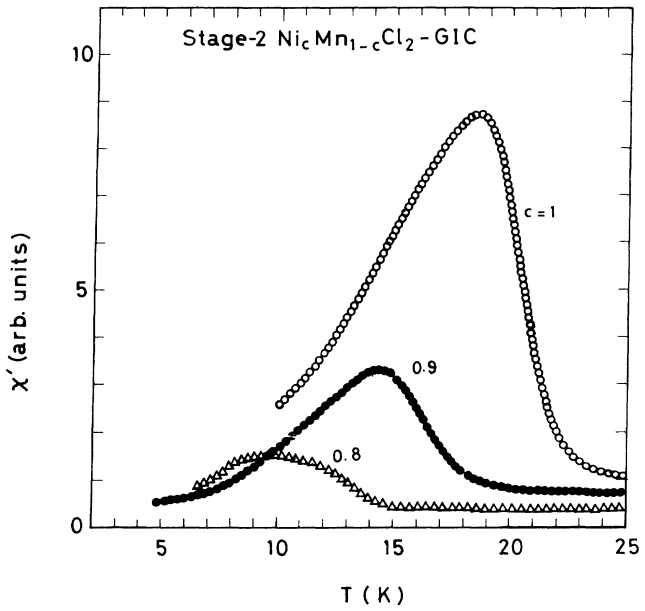

FIG. 5. Real part of ac magnetic susceptibility (χ') vs T for stage-2 $Ni_cMn_{1-c}Cl_2$ GIC's with $c=0.8$, 0.9, and 1.0. An ac magnetic field of $\nu=330$ Hz and $h=300$ mOe is applied along the c plane.

$$M(T)=A\int_T^{\infty}\left[1-\frac{T}{T_c}\right]^{\beta}f(T_c)dT_c\ , \tag{5}$$

with

$$f(T_c)=\frac{1}{\sqrt{2\pi}\sigma}\exp\left[-\frac{1}{2}\left[\frac{T_c-\langle T_c\rangle}{\sigma}\right]^2\right], \tag{6}$$

where A is a constant. The least-squares fit of M/H vs T of Fig. 4(a) to Eq. (5) yields the values of $\langle T_c \rangle$, σ, and β listed in Table III. The value of β seems to be independent of Ni concentration at least for $0.7 \le c \le 1$: $\beta \approx 0.25$. Figure 4(b) shows the temperature dependence of M/H at $H=840$ Oe for stage-2 $Ni_cMn_{1-c}Cl_2$ GIC's with $c=0.2$, 0.3, and 0.4. The magnetization monotonically decreases with decreasing temperature, indicating no magnetic phase transition, at least above 1.5 K.

The magnetic phase transition of stage-2 $Ni_cMn_{1-c}Cl_2$ GIC's with $c=0.7$, 0.8, 0.9, and 1 was investigated by ac magnetic-susceptibility measurement in the temperature range $2.6 \le T \le 25$ K. Figure 5 shows the temperature dependence of the real part of the ac magnetic susceptibility χ' of stage-2 $Ni_cMn_{1-c}Cl_2$ GIC's with $c=0.8$, 0.9, and 1. The real part χ' shows a broad peak at the critical

TABLE III. Critical exponent β, distribution width of critical temperature, σ, average critical temperature $\langle T_c \rangle$, and critical temperature T_c for stage-2 $Ni_cMn_{1-c}Cl_2$ GIC's.

c	β	σ (K)	$\langle T_c \rangle$ (K)	T_c (K)
0.7	0.275	1.218	6.954	5.31
0.8	0.262	1.154	11.570	9.58
0.9	0.290	1.669	16.020	14.34
1	0.241	1.869	21.051	18.38

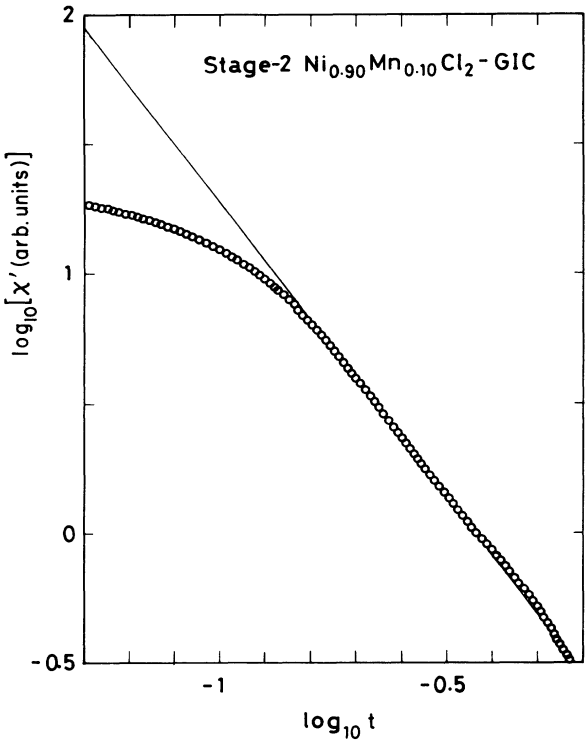

FIG. 6. Log-log plot χ' vs t $(=T/T_c-1)$ for the stage-2 $Ni_cMn_{1-c}Cl_2$ GIC with $c=0.90$. The solid line denotes a least-squares fit to a power law with $\gamma=2.27$.

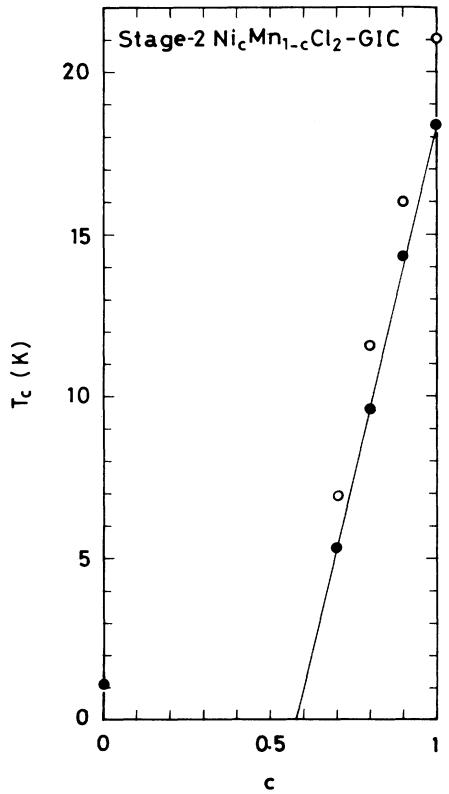

FIG. 7. Critical temperature T_c vs c for stage-2 $Ni_cMn_{1-c}Cl_2$ GIC's which are determined from the ac magnetic-susceptibility (●) and magnetization measurements (○). The solid line is a straight line with slope $d[\ln T_c(c)]/dc=2.38$.

temperature T_c listed in Table III. The critical temperature T_c shifts to the lower-temperature side with decreasing Ni concentration. The peak value of χ' rapidly decreases as the Ni concentration decreases and tends to reduce to zero for samples with $c \leq 0.7$. Figure 6 shows the log-log plot of χ' versus reduced temperature t $(=T/T_c-1)$ for $c=0.9$. In the temperature range $0.19 \leq t \leq 0.35$, the least squares fit of the data to the power law yields the critical exponent $\gamma=2.27\pm0.02$. For $t<0.19$ the slope of the curve $\log_{10}\chi'$ vs $\log_{10}t$ decreases with decreasing t, probably because of intrinsic behavior such as a crossover effect or a smearing of the critical temperature. The value of γ for $c=0.8$ is obtained as $\gamma=2.25\pm0.02$ in the temperature range $0.16 \leq t \leq 0.27$. These values of γ are likely to be close to that of the stage-2 $NiCl_2$ GIC: $\gamma=1.99\pm0.02$. Rogiers, Grundke, and Betts[13] have shown from a high-temperature series expansion of the 2D XY model that the susceptibility has a conventional power-law divergence with $\gamma=2.51\pm0.25$ rather than an exponential singularity. The value of γ in the stage-2 $Ni_cMn_{1-c}Cl_2$ GIC's, which is a little smaller than this theoretical value of γ, is indicative of the 2D XY character in the critical behavior of these compounds.

Figure 7 shows the critical temperature T_c vs Ni concentration for stage-2 $Ni_cMn_{1-c}Cl_2$ GIC's, where the critical temperatures denoted by solid and open circles are determined from ac susceptibility measurements at $H \approx 0$ and dc magnetic-susceptibility measurements at $H=100$ Oe, respectively. The values of T_c at $H=100$ Oe are larger than those at $H \approx 0$. This is consistent with a well-known result that the critical temperature of a 2D XY ferromagnet apparently shifts to higher temperatures when an external field H is applied along the direction of the easy axis.[14] For $c=0$, the stage-2 $MnCl_2$ GIC undergoes a phase transition at the Néel temperature $T_N=1.1$ K.[10,11] The critical temperature rapidly decreases with decreasing Ni concentration. The initial slope $\zeta=[d \ln T_c(c)/dc]$ at $c=1$ is obtained as $\zeta=2.38$.

IV. DISCUSSION

First, we discuss the magnetic phase diagram of stage-2 $Ni_cMn_{1-c}Cl_2$ GIC's. In Fig. 7 the critical temperature T_c rapidly decreases with an increase of Mn concentration and tends to reduce to zero around $c \approx 0.6$. Since the ferromagnetic interaction J(Ni-Ni) is much stronger than J(Ni-Mn), the role of Mn^{2+} ions may not be different from that of the diamagnetic ions in the Ni-rich concentration region. A continuous replacement of Ni^{2+} ions by Mn^{2+} ions results in a weakening of the ferromagnetic long-range order in the intercalate layer. The disappearance of ferromagnetic long-range order of Ni^{2+} spins below $c \approx 0.6$ can be confirmed from the Ni-concentration dependence of spontaneous magnetization. It is predicted from the percolation theory[15] that the Ni^{2+} ions belong either to 2D infinite networks or to finite clusters in the $Ni_cMn_{1-c}Cl_2$ intercalate layers with $c > c_p$, where c_p is a percolation threshold and is predicted as $c_p=0.5$ for the triangular lattice. Only the Ni^{2+} ions belonging to 2D infinite networks contribute to the magnetization per Ni mol, M_{Ni}. The fraction of the mag-

netization M_{Ni} to the saturation magnetization M_S, F, may be described by

$$F=\frac{M_{Ni}}{M_s}=\frac{N_0}{N}\ , \tag{7}$$

where N_0 is the number of Ni^{2+} ions belonging to 2D infinite networks, N is the total number of Ni^{2+} ions, and

$$M_s=N_A\mu_B g(\mathrm{Ni})S(\mathrm{Ni})$$
$$=1.262\times10^4\mathrm{emu/Ni\,mol}\ .$$

Figure 8 shows the fraction F vs Ni concentration at $T=4$ K and $H=100$ Oe for stage-2 $Ni_cMn_{1-c}Cl_2$ GIC's, where M_{Ni} is defined by M/c and the value of M is obtained from Fig. 4(a). The smaller value of F at $c=1$ than unity indicates that the magnetization does not saturate sufficiently at $T=4$ K and $H=100$ Oe. The value of F rapidly decreases with decreasing Ni concentration and is extrapolated to zero around $c\approx0.6$. This result indicates that the ferromagnetic long-range order may disappear below $c\approx0.6$. In Fig. 8, for comparison, we also show the fraction $F\ (=M_{Co}/M_s)$ vs Co concentration at $T=2$ K and $H=100$ Oe for stage-2 $Co_cMn_{1-c}Cl_2$ GIC's,[5] where

$$M_s=N_A\mu_B g(\mathrm{Co})S(\mathrm{Co})=1.787\times10^4\ \mathrm{emu/Co\ mol}\ ,$$

with $g(\mathrm{Co})=6.4$ and $S(\mathrm{Co})=\frac{1}{2}$. The fraction F gradually decreases with increasing Mn concentration and exhibits a noticeable tail even below $c_p=0.5$, indicating that the ferromagnetic long-range order of Co^{2+} spins does not vanish even below $c_p=0.5$. In Fig. 9 we show the data of

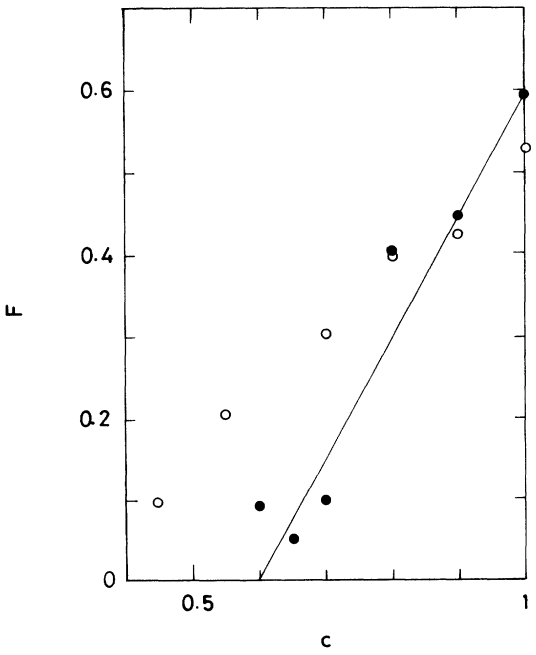

FIG. 8. Concentration dependence of fraction $F=M_{Ni}/M_s$ at $T=4$ K and $H=100$ Oe in stage-2 $Ni_cMn_{1-c}Cl_2$ GIC's (●) and $F=M_{Co}/M_s$ at $T=2$ K and $H=100$ Oe in stage-2 $Co_cMn_{1-c}Cl_2$ GIC's [Suzuki *et al.* (Ref. 5)] (○). The solid line is a guide to the eye.

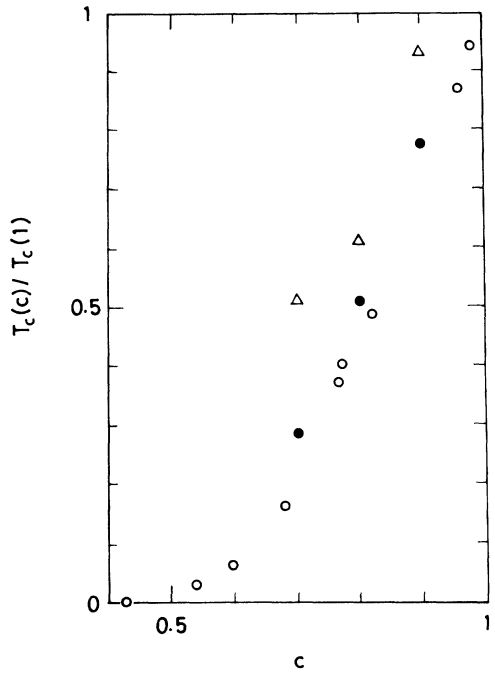

FIG. 9. $T_c(c)T_c(1)$ vs c for stage-2 $Ni_cMn_{1-c}Cl_2$ GIC's (●) (present work), stage-2 $Co_cMn_{1-c}Cl_2$ GIC's (△) [Suzuki *et al.* (Ref. 5)], and $K_2Cu_cZn_{1-c}F_4$ (○) [Okuda *et al.* (Ref. 17)].

$T_c(c)/T_c(1)$ versus concentration c for stage-2 $Ni_cMn_{1-c}Cl_2$ GIC's, stage-2 $Co_cMn_{1-c}Cl_2$ GIC's,[16] and $K_2Cu_cZn_{1-c}F_4$.[17] The value of $T_c(c)/T_c(1)$ for the stage-2 $Co_cMn_{1-c}Cl_2$ GIC's is larger than that for the stage-2 $Ni_cMn_{1-c}Cl_2$ GIC's for $c\geq0.7$, which is consistent with the above result that the critical concentration, below which the ferromagnetic long-range order of Co^{2+} in stage-2 $Co_cMn_{1-c}Cl_2$ GIC's disappears, is lower than that of Ni^{2+} in stage-2 $Ni_cMn_{1-c}Cl_2$ GIC's ($c\approx0.6$).

Here we note that the interaction J(Co-Mn) in stage-2 $Co_cMn_{1-c}Cl_2$ GIC's is almost the same as J(Ni-Mn) in stage-2 $Ni_cMn_{1-c}Cl_2$ GIC's. The different concentration dependence of F around $c=0.5$–0.6 in stage-2 $Ni_cMn_{1-c}Cl_2$ GIC's and $Co_cMn_{1-c}Cl_2$ GIC's may be ascribed to the difference of the spin symmetry in the stage-2 $NiCl_2$ GIC and $CoCl_2$ GIC. In the stage-2 $NiCl_2$ GIC, the Ni-Ni interactions are predominantly of Heisenberg character, while in the stage-2 $CoCl_2$ GIC the Co-Co interactions are of largely XY character. In fact, the inplane spin Hamiltonian of the stage-2 $CoCl_2$ GIC is described by

$$H=-2J\sum_{\langle i,j\rangle}\mathbf{S}_i\cdot\mathbf{S}_j+2J_A\sum_{\langle i,j\rangle}S_i^zS_j^z\ , \tag{8}$$

where J(Co-Co) (=7.75 K) is the ferromagnetic intraplanar exchange interaction and J_A(Co-Co) (=3.72 K) is the anisotropic exchange interaction. The XY anisotropy parameter of the stage-2 $CoCl_2$ GIC, η(Co-Co), is much larger than that of the stage-2 $NiCl_2$ GIC, η(Ni-Ni):

$$\eta(\mathrm{Co\text{-}Co})=J_A(\mathrm{Co\text{-}Co})/J(\mathrm{Co\text{-}Co})=0.48$$

and

$$\eta(\text{Ni-Ni})=D(\text{Ni})/2zJ(\text{Ni-Ni})=7.62\times10^{-3} .$$

It is qualitatively understood from the following simple model[18] that the value of $T_c(c)/T_c(1)$ decreases more rapidly with dilution for the Heisenber-like system than for the XY-like system. For $c\approx c_p$ the infinite cluster is represented in terms of weakly coupled 1D chains with intrachain interaction J_0 and interchain interaction J_1. The critical temperature T_c is determined by equating the thermal energy k_BT to the interaction energy between nearest-neighbor spins in adjacent chains, $k_BT=\xi_{1D}(T_c)|J_1|S(S+1)$, where the intrachain correlation length $\xi_{1D}(T)$ is given by $\xi_{1D}(T)=2|J_0|S(S+1)/k_BT$ for Heisenberg symmetry and $\xi_{1D}(T)=4|J_0|S(S+1)/k_BT$ for XY symmetry. Then it follows that the critical temperature T_c^{XY} for the system with XY symmetry is lower than T_c^H for the system with Heisenberg symmetry: $T_c^{XY}/T_c^H=\sqrt{2}$.

From the above discussion we can conclude that the T_c-vs c curve of stage-2 $Ni_cMn_{1-c}Cl_2$ GIC's agrees well with the phase boundaries of diamagnetically diluted systems. It is well known that the initial slope of $T_c(c)/T_c(1)$ vs c, ζ, strongly depends on the dimensionality and spin symmetry of system. In Fig. 9 the initial slope of stage-2 $Ni_cMn_{1-c}Cl_2$ GIC's ($\zeta=2.38$) is a little smaller than that of $K_2Cu_cZn_{1-c}F_4$ ($\zeta\approx3$).[17] Note that the in-plane spin Hamiltonian of K_2CuF_4 is also described by Eq. (8) with J(Cu-Cu) (=11.93 K) and J_A(Cu-Cu) (=0.09 K).[19] The XY spin anisotropy parameter of K_2CuF_4 is almost the same as that of stage-2 $NiCl_2$ GIC's:

$$\eta(\text{Cu-Cu})=J_A(\text{Cu-Cu})/J(\text{Cu-Cu})=7.54\times10^{-3} .$$

The large initial slopes observed in stage-2 $Ni_cMn_{1-c}Cl_2$ GIC's and $K_2Cu_cZn_{1-c}F_4$ may be closely related to the fact that these systems magnetically behave like a 2D Heisenberg ferromagnet with very small XY anisotropy. Stinchcombe[20] has shown from a position-space renormalization-group method that the dependence of T_c on Ising anisotropy δ and concentration c is described by

$$\frac{T_c(c,\delta)}{J}\sim\frac{2c-1}{\mu\ln(1/\delta)} \quad \text{as } (\delta\to0) , \tag{9}$$

with $\mu=0.21$, where the spin Hamiltonian of the pure system is given by

$$\mathcal{H}=-2J\sum_{\langle i,j\rangle}[(1-\delta)(S_i^xS_j^x+S_i^yS_j^y)+S_i^zS_j^z] . \tag{10}$$

From Eq. (9) the initial slope of this system is estimated as $\zeta=2$ and is independent of the Ising spin anisotropy δ in the limit of $\delta\approx0$. With increasing Ising anisotropy δ, the initial slope ζ is predicted to decrease rapidly from $\zeta=2$, approaching that for the 2D Ising model. McGurn[21] has predicted from a random-phase approximation that the initial slope for the system with the spin Hamiltonian of Eq. (10) takes the value of $\zeta=3.14$ for the isotropic limit of $\delta\approx0$, which is much larger than the value predicted by Stinchcombe.[20] In spite of different values in ζ between these two theories, it may be understood that the large value of ζ is characteristic of the 2D Heisenberg system with small Ising anisotropy. As far as we know, there has been no theory for the initial slope in a 2D Heisenberg ferromagnet with XY anisotropy. However, the initial slope for the 2D Heisenberg ferromagnet with small XY anisotropy is expected to be a little smaller than that for a 2D Heisenberg ferromagnet with small Ising anisotropy because of the monotonic decrease of initial slope with the lowering of spin symmetry.

In contrast to the phase diagram for the Ni-rich concentration, the magnetic phase diagram in the Mn-rich concentration is not established at all because of lack of experimental data. In this concentration region there may occur a competition between the antiferromagnetic interaction J(Mn-Mn) and ferromagnetic interaction J(Ni-Mn), which gives rise to a spin-frustration effect. A continuous replacement of Mn^{2+} ions by Ni^{2+} ions results in a weakening of the antiferromagnetic long-range order in the intercalate layer. This antiferromagnetic long-range order may disappear around $c\approx0.22$, where the Curie-Weiss temperature becomes zero.

V. CONCLUSION

The magnetic phase transition of stage-2 $Ni_cMn_{1-c}Cl_2$ GIC's has been studied by dc and ac magnetic-susceptibility measurements. The magnetic phase diagram has been determined for $c\geq0.6$ and $c=0$. It becomes clear that a Ni-rich ferromagnetic phase is built up by the Ni^{2+} ions, whereas the Mn-rich antiferromagnetic phase may be formed by Mn^{2+} ions at least at $c\approx0$. The ferromagnetic and antiferromagnetic phases are separated by a paramagnetic phase. The Ni^{2+} and Mn^{2+} spins do not take part in the magnetic long-range order of the Ni^{2+} and Mn^{2+} networks, respectively. Thus the magnetic behavior of this system can be explained by percolation effects. In the present work, no spin-glass phase is observed at temperatures above 2.6 K. However, there may be still a possibility of a spin-glass phase at low temperature around $c\approx0.22$, because of the competition between ferromagnetic J(Ni-Mn) and antiferromagnetic interactions J(Mn-Mn).

ACKNOWLEDGMENTS

We would like to thank H. Suematsu and Y. Hishiyama for providing us with high-quality single-crystal Kish graphites. We are grateful to W. Brinkman for his help on the dc and ac magnetic-susceptibility measurements. This work was supported by National Science Foundation Grant No. DMR-8902351.

[1]M. Yeh, M. Suzuki, and C. R. Burr, Phys. Rev. B **40**, 1422 (1989).
[2]M. Yeh, I. S. Suzuki, M. Suzuki, and C. R. Burr, J. Phys. Condens. Matter **2**, 9821 (1990).
[3]J. T. Nicholls and G. Dresselhaus, Phys. Rev. B **41**, 9744 (1990).
[4]M. Suzuki, L. F. Tien, I. S. Suzuki, and C. R. Burr, J. Appl. Phys. **67**, 5749 (1990).
[5]I. S. Suzuki, M. Suzuki, L. F. Tien, and C. R. Burr, Phys. Rev. B **43**, 6393 (1991).
[6]H. Suematsu, R. Nishitani, R. Yoshizaki, M. Suzuki, and H. Ikeda, J. Phys. Soc. Jpn. **52**, 3874 (1983).
[7]M. Suzuki, H. Ikeda, and Y. Endoh, Synth. Met. **8**, 43 (1983).
[8]M. Suzuki, K. Koga, and Y. Jinzaki, J. Phys. Soc. Jpn. **53**, 2745 (1984).
[9]D. G. Wiesler, M. Suzuki, P. C. Chow, and H. Zabel, Phys. Rev. B **34**, 7951 (1986).
[10]Y. Kimishima, A. Furukawa, M. Suzuki, and H. Nagano, J. Phys. C **19**, L43 (1986).
[11]M. Matsuura, Y. Karaki, T. Yonezawa, and M. Suzuki, Jpn. J. App. Phys. **26**, Suppl. 26-3, 773 (1987).
[12]T. Hashimoto, J. Phys. Soc. Jpn. **18**, 1140 (1963).
[13]J. Rogiers, E. W. Grundke, and D. D. Betts, Can. J. Phys. **57**, 1719 (1979).
[14]M. Suzuki and H. Ikeda, J. Phys. Soc. Jpn. **50**, 1133 (1981).
[15]See, for example, A. Coniglio, in. *Magnetic Phase Transitions,* edited by M. Ausloos and R. J. Elliott (Springer-Verlag, New York, 1983), p. 195.
[16]M. Suzuki, I. S. Suzuki, F. Khemai, and C. R. Burr, J. Appl. Phys. **70**, 6098 (1991).
[17]Y. Okuda, Y. Tohi, I. Yamada, and T. Haseda, J. Phys. Soc. Jpn. **49**, 936 (1980).
[18]L. J. de Jongh, in *Magnetic Phase Transitions,* edited by M. Ausloos and R. J. Elliott (Springer-Verlag, New York, 1983), p. 172.
[19]K. Hirakawa, J. App. Phys. **53**, 1893 (1982).
[20]R. B. Stinchcombe, J. Phys. C **14**, 397 (1981).
[21]A. R. McGurn, J. Phys. C **12**, 3523 (1979).